Influence of ion velocity on damage efficiency in the single ion-target irradiation system: Au-$Bi_2Sr_2CaCu_2O_x$

D. X. Huang* and Y. Sasaki
Japan Fine Ceramics Center, 2-4-1 Mutsuno, Atsuta-ku, Nagoya 456-8587, Japan

Y. Ikuhara
Department of Materials Science, University of Tokyo, Tokyo 113, Japan

(Received 13 July 1998)

Based on the cross section measurement of the columnar defect along the ion path using high-resolution electron microscopy, we developed a method to study the influence of ion velocity on ion irradiation damage. The use of a single ion-target irradiation system avoids the influences of the different target materials and the different species of incident ions on the irradiation damage. By investigating the dependence of damage efficiency on the ion velocity, we can minimize the influence of the different ion effective charge on the ion irradiation damage. The application on the Au-$Bi_2Sr_2CaCu_2O_x$ system shows that there is a critical velocity $\nu_c \sim 0.057c$ (c, the velocity of light) at which the damage efficiency is maximum. By reanalyzing the previous published data, we have found a similar critical velocity ($\nu_c \sim 0.055c$) in the Xe-YIG (yttrium garnet) irradiation system, indicating it is a quite general phenomenon. From this observation, the irradiation damage process is divided into two stages. In the high ion velocity region the irradiation damage is ion velocity controlled and in the low ion velocity region the irradiation damage is the energy-density threshold controlled. The peak of damage efficiency corresponds to the turning point between two stages. [S0163-1829(99)00605-0]

I. INTRODUCTION

Ion irradiation has become a most effective method to artificially create crystal defects for flux pinning and prominently enhance the critical current density (J_c) in superconducting materials.[1–7] The irradiation-induced defect morphology, which greatly influences the efficiency of flux pinning, is mainly controlled by the specific energy deposition process of incident ions in the target material. In the high-energy region (>100 keV/amu), the incident ion deposits its energy in the target material mainly through the interaction with the target electrons, which is called electronic stopping power. The ion energy deposited electronically is very quickly transferred from the target electrons to the lattice and then a damage (irradiation-induced defect) will be produced in the target material. The common defects induced by high-energy ions are columnar defects with amorphous cores in superconducting materials.[2,8–11]

In the formation of irradiation damage, stopping power (dE/dx) is usually used as a main parameter for analyzing the origin for the change of damage morphology. Since the irradiation damage is due to a certain amount of ion energy rapidly deposited in a localized area in the target material, it is very easy to understand the importance of dE/dx in the irradiation damage process as it gives the amount of the deposited energy in a unit length of ion path. However, for such a complicated physical process as the irradiation damage process, it is hard to be completely described by only one physical parameter.

In the last ten years, several research groups in France intensively studied the irradiation-damage process using several kinds of heavy ions with different ion energies in ferrimagnetic yttrium garnet (YIG).[12–26] By summarizing their experiment data, they found that the electronic stopping power dE/dx was not the only key parameter and the ion velocity also plays a very important role in the formation of irradiation damage.[23,25] For the same value of dE/dx, the damage cross section (A) produced by the low-velocity ion was systematically higher than that produced by the high-velocity ion in a large range of dE/dx. Since the irradiation damage process is closely related to the species of incident ion, it is very difficult to have a full understanding for the detailed influence of ion velocity on the damage process by analyzing the mixed experimental data produced by different kinds of incident ions.

Plan-view methods such as chemical etching (CE),[27] conversion electron Mössbauer spectroscopy (CEMS),[28] channeling Rutherford backscattering spectrometry (CRBS)[29] and plan-view electron microscopy[10] have been widely used to investigate the irradiation damage morphology in the irradiated materials. Using the above methods, for one irradiation sample only one damage-cross-section datum can be obtained. For analyzing the influence of ion velocity on the damage cross section, we have to do a large amount of irradiation experiments. It is both time consuming and expensive. Recently we reported a continuous cross-sectional TEM observation method by which we can effectively acquire a series of damage-cross-section data in a large ion velocity range by one ion-irradiated sample.[30] This method also gives us a possibility to study the dependence of damage cross section on ion velocity in a much simplified system, single ion-target irradiation system. Since the ion species and the target material are both fixed in the single ion-target irradiation system, we no longer need to consider how the damage cross section is influenced by the different electronic density distribution and the different crystal structure. Also we do not need to consider how the damage cross section is influ-

enced by the different species of incident ion and by the different incident direction of the ion beam with respect to the target crystal. Along the ion path, the difference for the damage cross section in two different ion penetration depth regions only results from the different value of ion velocity and the different value of ion effective charge in these two depth regions. Since the ion effective charge has a simple functional relation with the ion velocity,[31] therefore, if the selected physical parameter is suitable the influence of the ion effective charge on the irradiation damage process can be minimized. Finally, we can study the pure influence of ion velocity on the irradiation damage process using a single ion-target irradiation system.

In this study, the damage cross-section A in each penetration depth in the 230-MeV Au-irradiated $Bi_3Sr_2CaCu_2O_x$ crystal was estimated by cross-sectional high-resolution electron microscopy (HREM). Instead of the damage cross section A, the damage efficiency $\varepsilon(\varepsilon = A/dE/dx)$ was used to describe the amount of damage in the target material. The influence of ion effective charge in the damage process was minimized. By combining with two previously reported data in the same ion-target system, then we successfully carried out an investigation for the pure influence of ion velocity on the irradiation damage process. Using the same research method suggested in this study, we reanalyzed the existent experimental data for YIG irradiated by several kinds of ions. The obtained results for these two kinds of ion-target systems were further compared. Finally, a two-stage model has been suggested to explain the experimental results.

II. EXPERIMENTS AND ANALYSIS METHODS

A. Ion irradiation and TEM observation

The $Bi_2Sr_2CaCu_2O_x$ crystal sheet with a thickness of about 20 μm has been used for the present irradiation experiment. The surface of the crystal sheet is a cleaved a-b plane of the $Bi_2Sr_2CaCu_2O_x$ crystal. A 230-MeV Au ion beam was used to bombard the crystal sheet at room temperature with an incident direction perpendicular to the sample surface. The incident Au^{14+} ions were produced in a Tandem accelerator at the Japan Atomic Energy Research Institute. The used ion dose in our experiments was about 9.7×10^{10} ions/cm^2. A standard method was used to prepare cross-sectional TEM specimens for the further TEM analyses. A series of low- and high-resolution images were taken along the ion penetration path using a Topcon EM-002B high-resolution TEM (HREM, 200 keV) with a point-to-point resolution of 0.18 nm.

B. Measurement of damage efficiency

The damage cross section A in each penetration depth region was measured by the high-resolution TEM images taken in the corresponding depth region. The detailed steps for the measurement are described as follows. First, using the cross-sectional HREM observation method, we can obtain many sectional images for the columnar defects produced by different incident ions in each depth region. Next, from the obtained HREM images we can accurately measure the size of amorphous area in each columnar defect. Then, the damage diameter (D) in each depth region can be obtained by averaging all the values of the measured columnar-defect sizes in the same depth region. Supposing that the damaged area is a regular cylinder, the damage cross section A can be further calculated through the relation $A = \pi(D/2)^2$. Using a high-energy-extended EDEP-1 computer code,[32] we can calculate the value of stopping power dE/dx in each depth region. Consequently, the damage efficiency ε in each depth region can be obtained through the relation $\varepsilon = A/(dE/dx)$.

III. RESULTS AND DISCUSSIONS

A. How to analyze the effect of ion velocity

As mentioned above, many factors influence the damage cross section. In order to understand the detailed relationship between ion velocity and damage cross section, we have to simplify the research object. First, we should fix the target material. This is because the incident ion in the different target material has a different energy-deposition process and the dependence of damage cross section on ion velocity will also be different. Secondly, the different species of incident ion will result in a different changing process of the effective ion charge and further result in a different rate of ion energy deposition in the target material. It will also change the dependence of the damage cross section on ion velocity. Thus we should ideally fix the species of the incident ion. Thirdly, the different ion velocity will certainly result in a different value of dE/dx. We all know that the damage cross section of an energetic ion in the target material is strongly influenced by the value of dE/dx. Therefore, for the same ion with two different values of velocity, the difference of the produced damage cross section will result from two reasons. The first is the direct influence of ion velocity. The second is the indirect influence of ion velocity through the change of dE/dx induced by the different value of ion velocity. Two reasons are mixed together and very difficult to separate. Therefore, if we simply investigate the changing relation of the damage cross section with ion velocity, we can hardly distinguish that the change of the damage cross section is caused by the difference of ion velocity or by the difference of the dE/dx value. The damage efficiency (ε), however, seems more appropriate than the damage cross section for investigating the influence of ion velocity on the process of irradiation damage. This is because ε is the damage cross section per unit dE/dx and it only includes the high-order influence of dE/dx on the damage cross section. Therefore, to study the changing process of damage efficiency against ion velocity can help us to reveal the direct influence of ion velocity on the process of irradiation damage more clearly. Based on the above three points, to investigate the effect of ion velocity in the process of irradiation damage, we should select a single ion-target irradiation system and start the investigations from analyzing the changing process of damage efficiency with the incident ion velocity.

B. Experimental measurements of damage efficiency

A series of HREM images for the irradiation-induced columnar defects have been taken continuously along the ion penetration path. Figure 1 shows four pieces of typical images picked out from them. From this figure, we can see that the diameter of the damaged amorphous cylinder gradually

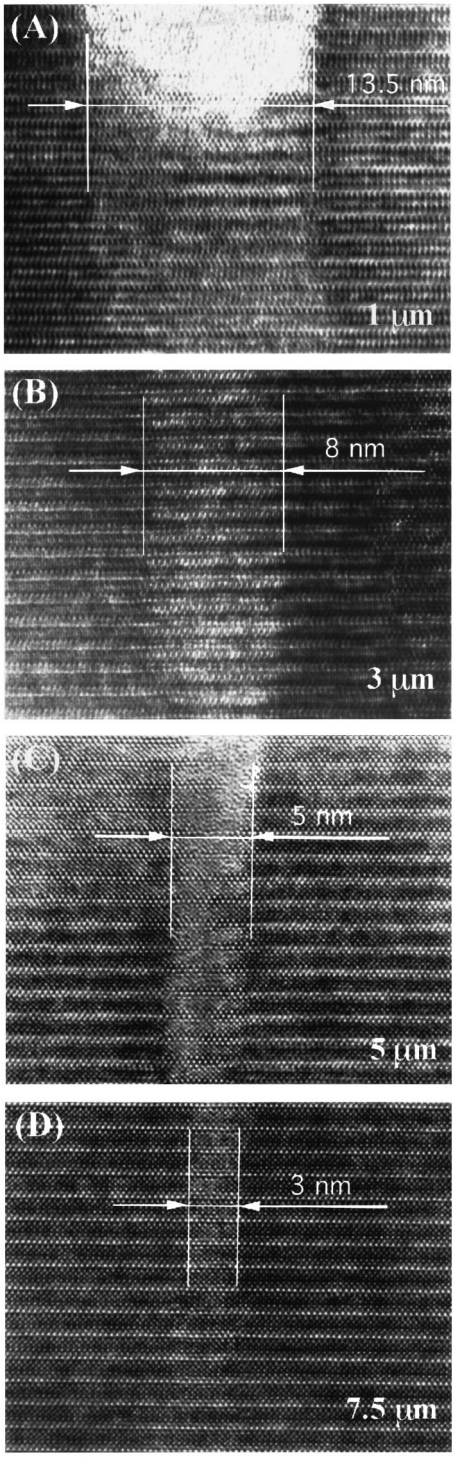

FIG. 1. HREM images respectively taken at penetration depths of about (a) 1 μm, (b) 3 μm, (c) 5 μm, and (d) 7.5 μm along the ion path, showing the change of the columnar defect size with the penetration depth.

decreases from 13.5 to 3 nm when the penetration depth of the incident Au ion in the target changes from 1 to 7.5 μm.

The damage cross section and the corresponding damage efficiency in each penetration depth region were estimated using the method introduced above. The values of the stopping power, the residual ion energy, and the relative ion velocity in each penetration depth region were all calculated by the EDEP-1 computer code.[32] All the measured data, calculated data, and two previously reported data[10,11] for the same ion-target irradiation system have been summarized and shown in Table I.

C. Effect of ion velocity on the irradiation damage process

1. In the multiple-ion-target system

A few years ago, Meftah *et al.*[21] analyzed the changing relation of damage efficiency with the stopping power dE/dx by summarizing the experimental data in YIG irradiated by several kinds of energetic heavy ions. The results indicated that the damage efficiency in the low-ion-velocity region was systematically higher than the damage efficiency in the high-ion-velocity region for the same value of dE/dx. The plateau of damage efficiency in the high dE/dx region for the high-velocity-ion irradiation did not appear again for the low-velocity-ion irradiation in the same dE/dx region. Instead, for the low-velocity-ion irradiation, there was a peak value for the damage efficiency in the high dE/dx region. When the dE/dx becomes higher and higher, the damage efficiency does not keep constant and decreases gradually.

Using the data summarized by Meftah *et al.*,[25] we plotted another damage efficiency curve against the ion velocity v, which is shown in Fig. 2. Since the experiment data are too scattered, it is very difficult to obtain the detailed changing relation of damage efficiency with the ion velocity from such a ε-ν curve. However, we can see the tendency for the change of damage efficiency with the ion velocity. From this curve, we can find that the damage efficiency increases systematically when the ion velocity decreases gradually. As indicated by the solid dots, there are three specific data in Fig. 2, which have a large deviation from the general changing law of damage efficiency with ion velocity. These three data were obtained from the Ar-, S-, and F-ion irradiation experiments. We can see that all three kinds of ions are much lighter than the ions usually used to bombard the YIG crystal, e.g., Xe, Kr, Pb, and U ions. This indicates that the damage process in the light-ion irradiation case will be much different from that in the heavy-ion irradiation case. Concerning the damage behaviors for the light-ion irradiation, it will be the main topics for our next paper.[33]

2. In the single ion-target system

Using a single ion-target irradiation system Au-$Bi_2Sr_2CaCu_2O_x$, we investigated the effect of ion velocity on the irradiation damage process. Figure 3 shows a curve of damage efficiency versus ion velocity in electronic stopping power region by using the measured data in this study and combining with two previous data[10,11] in the same ion-target irradiation system. As shown by this curve, in the high-velocity region, the damage efficiency increases with the decrease of ion velocity along the ion penetration path, which is very similar with the results obtained in the multiple ion-target irradiation system in last section. When the ion velocity decreases to some value around $0.057c$, however, the damage efficiency reaches a maximum value. Then, as the ion velocity decreases further in the region of ion velocity less than $0.057c$, the damage efficiency turns to decrease gradually. There is a peak of damage efficiency on the ε-ν curve in the low-velocity region.

TABLE I. Experimental data measured by the HREM method in Au-irradiated $Bi_2Sr_2CaCu_2O_x$ single crystals. D and A are the damage diameter and damage cross section, respectively. ε is damage efficiency calculated by the formula of $\varepsilon = A/(dE/dx)$.

Target	Ion	Energy (MeV)	Energy (MeV/amu)	dE/dx (keV/nm)	D (nm)	A (nm^2)	Relative velocity v/c	ε (nm^3/keV)	Ref.
Bi-2212	Au	2640	13.4	38.5	7.1	39.59	0.169	1.03	26
	Au	300	1.52	31.5	16	201.06	0.057	6.38	25
	Au	200	1.02	28.8	13	132.73	0.047	4.61	
	Au	172	0.87	27.2	10	78.54	0.043	2.89	
	Au	120	0.61	23.8	7	38.48	0.036	1.62	
	Au	98	0.5	21.9	6	28.27	0.032	1.29	
	Au	77	0.39	19.8	4.8	18.1	0.029	0.91	
	Au	59	0.3	17.3	3.6	10.18	0.025	0.59	
	Au	50	0.25	15.9	2.8	6.16	0.023	0.39	

It is interesting that when we pick out all the reported experimental data for YIG irradiated by the same ion source, e.g., Xe, and plot a ε-v curve, we can also find a similar peak in the low-ion-velocity region. The corresponding value of ion velocity for this peak of ε in Xe-irradiated YIG is about $0.055c$, which we can also see in Fig. 3. All of these give us the important information that the appearance of the ε peak in the low-velocity region is a general phenomenon existing in the process of irradiation damage. The detailed data for the Xe-YIG irradiation system, which were picked up from the data summarized by Mefath *et al.*,[25] are shown in Table II.

D. The origin of the ε peak in the low-velocity region

1. A consideration from the threshold of dE/dx

It is known that there is an energy threshold for permanently moving an atom away from its lattice site. The detailed value of this energy is different for the different target crystal. When the energy supplied from outside is lower than this energy threshold, the atom will only have a vibration around its lattice site and never be moved away permanently. In the damaged area by ion irradiation, the target crystal is found to be amorphized. This means that there are a large number of target atoms that are moved permanently from their own places by the energy deposited from incident ions. Because the energy threshold exists for moving one atom from its lattice site, to move a large number of atoms, e.g., in the case of irradiation damage, an energy threshold should also exist.

Actually, many attempts have already been made to try to experimentally estimate the values of some important energy thresholds for generating different damage morphologies by ion irradiation in different target materials.[21,23,26,30,34–36] For ion-irradiated $Bi_2Sr_2CaCu_2O_x$ crystals, a threshold of dE/dx (S_c) for producing a continuous columnar defect was suggested by Leghissa *et al.*[35] and by Kumakura *et al.*[36] Recently, we further confirmed that the value of this threshold is about 16 keV/nm in the Au-ion irradiation case by cross-sectional TEM observation.[30] We believe that the existence of damage threshold is the reason for the limit on the in-

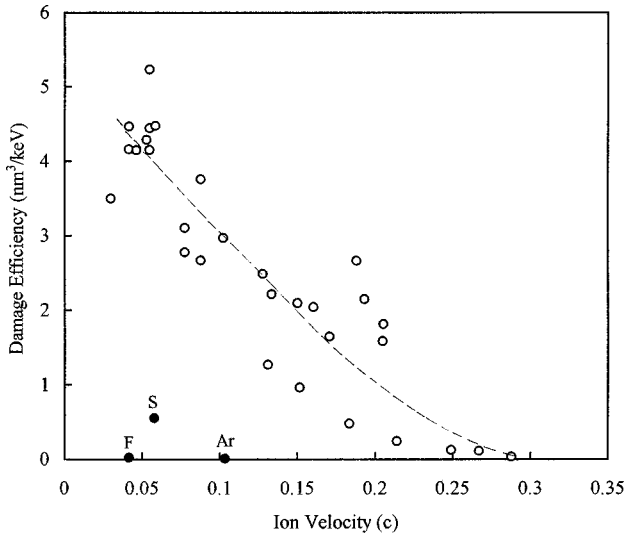

FIG. 2. Dependence of damage efficiency on ion velocity in YIG irradiated by many kinds of incident ions. The circles give out the data obtained in heavy ion irradiation experiments. The solid dots show the data obtained in light ion irradiation experiments. The characters near each solid dot show the detailed species of the incident ion.

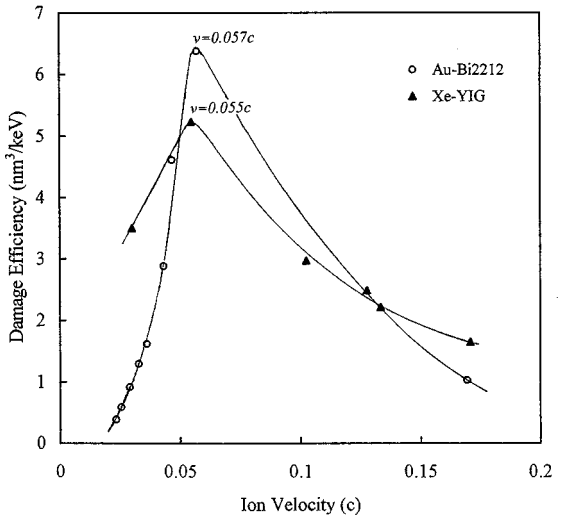

FIG. 3. Dependence of damage efficiency on ion velocity in single ion-target irradiation system. All circles are for the Au-$Bi_2Sr_2CaCu_2O_x$ ion-target system and all solid triangles are for the Xe-YIG system.

TABLE II. Experimental data for YIG irradiated by Xe ions with different ion velocities picked out from the summarized data by Meftah *et al.* (Ref. 21). D and A are the damage diameter and damage cross section, respectively. ε is damage efficiency calculated by the formula of $\varepsilon=A/(dE/dx)$.

Target	Ion	Energy (MeV/amu)	dE/dx (keV/nm)	D (nm)	A (nm^2)	Relative velocity v/c	ε (nm^3/keV)	Ref.
YIG	Xe	19.6	19	6.2	30.19	0.205	1.59	21
	Xe	17.4	20	7.4	43.01	0.193	2.15	21
	Xe	13.6	22	6.8	36.32	0.171	1.65	21
	Xe	8.3	25	8.4	55.42	0.133	2.22	21
	Xe	7.6	25.6	9	63.62	0.128	2.49	21
	Xe	4.9	27.5	10.2	81.71	0.102	2.97	21
	Xe	1.4	24.6	12.8	128.68	0.055	5.23	21
	Xe	0.42	19	9.2	66.48	0.03	3.5	21

crease of damage efficiency as the ion slows down in the low-velocity region. We all know that as an incident ion penetrates a target crystal, it will lose its energy on its penetration path and slow down gradually. The corresponding stopping power dE/dx for this slowing ion will also decrease gradually. When the dE/dx decreases to a value less than the threshold S_c, there will no longer be any columnar defects that can be observed by TEM. As the dE/dx decreases further, there will not be any damage that can be produced by such an incident ion. This means that the damage cross section A in this case will be zero. As a result, the damage efficiency $\varepsilon=A/(dE/dx)$ should also be zero. It is easy to imagine that as the ion velocity decreases further and further, a turning point (v_c) must appear for the damage efficiency changing from continuously increasing to a value of zero. Therefore, when we consider that the given dE/dx threshold existed in the formation of irradiation damage, the changing process of damage efficiency with ion velocity can be simply described as follows. First, when the ion velocity is larger than the turning point v_c, the damage efficiency increases with the decrease of ion velocity. Second, as the ion velocity gradually decreases to be smaller than v_c, the damage efficiency will decrease as the ion slows down. Finally, when the ion velocity decreases to some value, the dE/dx reaches its lower limit for producing damage in the target crystal. The damage efficiency will reach a value of zero. The damage-efficiency peak on the measured ε-ν curve experimentally confirmed the existence of this kind of turning point in the irradiation-damage process.

2. A consideration from the radial distribution of the deposited-energy density

We all know that the irradiation damage is due to the energy deposition of the energetic ions in the target materials. It is very easy to understand that the stopping power (dE/dx) is one key parameter to analyze the irradiation damage process, which gives the total deposited energy per unit length of path. However, dE/dx only can give a linear description for the ion-energy-deposition process in the target crystal. It does not provide any information to understand the radial distribution of the deposited energy density around the ion penetration path. As a result, in the description of damage morphology using dE/dx, we had a lot of trouble. For example, the irradiation-induced defect size is radically not a single-value function to dE/dx. It means that, for the same irradiation system, the same dE/dx can produce two kinds of columnar defects with different sizes, depending on the ion velocity. If dE/dx is the same, the higher the velocity, the smaller the size of the produced columnar defect. Also for a given columnar defect size, in the same ion-target system there are two kinds of dE/dx values corresponding to it. As an example to produce a columnar defect of 7 nm in diameter in the Au-irradiated $Bi_2Sr_2CaCu_2O_x$ crystal, we can use both the Au ion with a velocity of $0.169c$ (Ref. 11) and the Au ion with a velocity of $0.036c$ (Ref. 30) to bombard the target. The corresponding values of dE/dx are much different. For the ion with a velocity of $0.169c$, the value of dE/dx is about 38.5 keV/nm and for the ion with a velocity of $0.036c$, the value of dE/dx is about 23.8 keV/nm.

As early as the late 1960's, Katz *et al.* already tried to theoretically predict the initial radial distribution of the deposited energy $D(r)$ around the ion path.[37] About fifteen years later, Zhang *et al.*[38] and Waligórski *et al.*[39] established an analytic formula to estimate $D(r)$ by fitting the available experimental data and the Monte Carlo simulation results. The circle-dotted curve in Fig. 4 shows an example of the calculated radial distribution of the deposited energy $D(r)$ using above method in 200-MeV Au-irradiated $Bi_2Sr_2CaCu_2O_x$ crystals. The corresponding ion velocity is $0.047c$.

As is the case for dE/dx, a threshold for the density of the deposited energy D_0 should also exist for producing permanent damage in the target crystals. On the $D(r)$-r curve as shown in Fig. 4, we can find a value of r, r_0, and the corresponding value of $D(r)$ equals D_0. When the value of r is larger than r_0, the value of $D(r)$ will be less than D_0. This means that there will be no damage that can be produced in the area where the radial distance from the ion path is larger than r_0. Therefore the distance of r_0 actually corresponds to the damage radius of the incident ion in the target crystal. According to the above analyses, not all the deposited ion energy that can be used to produce the damage in the target materials. Only when the $D(r)$ is higher than D_0 can this part of energy produce damage in the target crystals.

a. The explanation for the increase of damage efficiency with the decrease of ion velocity in high-velocity region. We calculated a series of $D(r)$-r curves with different ion velocities. From these curves we can directly find that the dis-

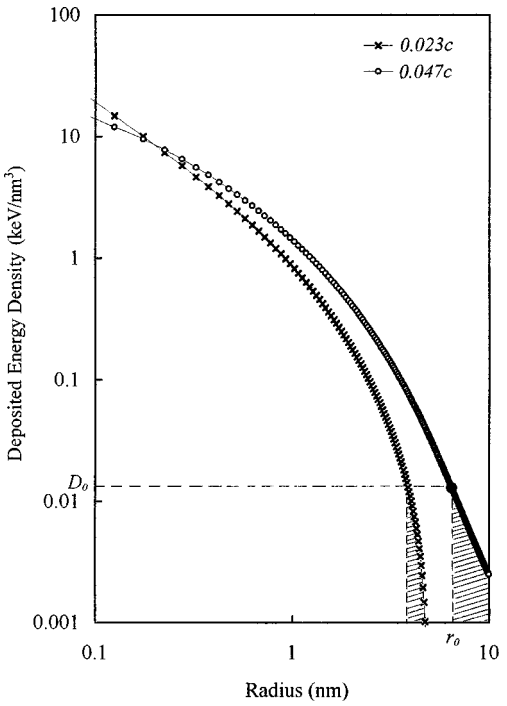

FIG. 4. The calculated radial distributions of deposited energy density in $Bi_2Sr_2CaCu_2O_x$ crystal for Au ions with velocities of $0.047c$ and $0.023c$, showing a more localized distribution of deposited energy for the ion with a relative lower velocity. For a given threshold of energy density D_0 to produce a permanent defect in the target, the corresponding damage radius r_0 can be estimated by this curve. The area difference between two shadow areas indicates that the amount of deposited energy distributed beyond the damaged area is larger for the ion with higher velocity.

tribution of deposited energy becomes more and more delocalized as the ion velocity increases gradually. The two example $D(r)$-r curves are shown in Fig. 4, briefly demonstrating the change tendency of $D(r)$ with the ion velocity. This indicates that when the ion velocity is higher, as shown by the shadowed area in Fig. 4, there is more energy that will be deposited in the area where the distance from the ion path is larger than r_0 and actually this part of energy has no contribution for producing permanent damage in the target. Therefore, for the same dE/dx, the damage efficiency will be lower for the incident ion with a relative higher velocity.

From the viewpoint of the interaction of a charged particle with target electrons, when the ion velocity is higher, the interaction between the incident ion and the target electron will be stronger. There will be more high-energy second electrons that can be excited in the interaction of the high-velocity ion with target electrons. This part of the high-energy electrons will carry a lot of energy and go far from the ion path. The part of the energy carried by high-velocity second electrons is usually useless for producing localized damage in the target material. Furthermore, as the ion velocity becomes higher and higher, more and more inner-shell electrons will be excited. Part of the energy of the excited inner-shell electron will be used to excite the outer-shell electron and the other part of energy will be released through hard x ray. Since the hard x ray is almost transparent for the target material and it can go much farther than the electrons, the part of energy carried by the hard x ray is also completely useless for producing localized damage in the target materials. Therefore, as the ion velocity increases, more and more ion energy will be deposited in the area far from the ion path and the damage efficiency will become lower and lower. The ε-ν curves in Figs. 2 and 3 experimentally reveal this change tendency of damage efficiency with the ion velocity in high-velocity region.

b. A two-stage model to explain the peak of damage efficiency in the low velocity region. According to above analyses, there are two main factors influencing the damage efficiency. One is the ion velocity. The second is the threshold of the deposited energy density for producing permanent damage in the target material. When the ion velocity is high, the deposited energy density is much larger than the energy density required to overcome this threshold. In this case, the delocalization of deposited ion energy due to the high ion velocity dominates the process of damage formation. Similar to the analyzed results in last section, the damage efficiency will increase with the decrease of ion velocity. However, in the low velocity region, the deposited energy density changes to be comparable with the energy density threshold. In this case, the damage efficiency is mainly controlled by the energy density threshold for producing permanent damage. When the ion velocity becomes lower, the total deposited energy will also become fewer. However, the energy threshold for producing damage in the target is a constant for a given target material and does not change with the ion velocity. This means that the lower velocity ion has to spend a relative higher ratio of its deposited energy to overcome the energy threshold to produce the damage in the same target material, that is to say, the damage efficiency will be lower. Finally, when the ion velocity is so low that almost all the deposited energy is used to overcome this energy density threshold, the damage efficiency in this case will equal zero. According to the viewpoint described above, the peak of damage efficiency appearing in low velocity can be understood as a turning point at which the damage efficiency changes from the ion velocity control to the deposited energy density control. Figure 5 is a schematic to briefly show the two stages for the changing process of damage efficiency with the ion velocity.

E. The effect of ion effective charge on the damage efficiency

It is known that the effective charge (Z^*) of the incident ion increases as the increase of ion velocity ν. The detailed relation between Z^* and ν was already suggested by Barkas in the early 1960's.[31] In the electronic energy loss region, we can approximately consider the target crystal as an electron aggregate with a given electron density. For a particle with a higher charge moving in this electron aggregate, the Coulombic resistance from the target electrons should be higher. This means that there will be more energy of the particle that is deposited in the target through the Coulombic interaction with the target electrons. As a result, the stopping power dE/dx should be higher. Since the dE/dx is influenced simultaneously by ion velocity and ion effective charge, it will be hard to clarify the pure effect of ion velocity on the irradiation damage through studying the changing relation of dE/dx with ion velocity.

However, according to the analytic formula suggested by Zhang[38] and Waligórski,[39] the radial distribution of depos-

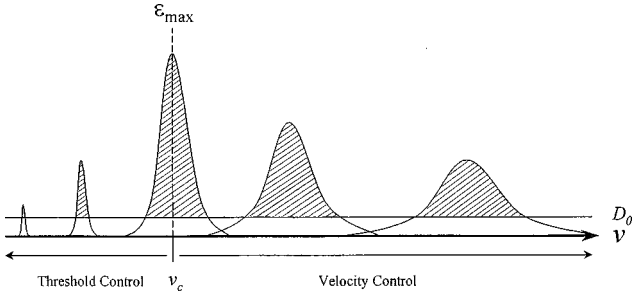

FIG. 5. A schematic showing the two-stage model in irradiation damage process. (1) Velocity controlled stage: For a given threshold of deposited energy density (D_0) to produce a permanent damage in a given target material, the damage efficiency (ε) decreases gradually with the increase of ion velocity in the high velocity region. This is because the higher velocity ion has a more delocalized distribution of deposited ion energy and the effective energy for producing damage as shown by shadow area is fewer relative to the total deposited ion energy. (2) Threshold controlled stage: Contrary to the case for high-velocity ions, the damage efficiency decreases with the decrease of ion velocity in the low velocity region. This is due to that the effective part of deposited energy for producing damage becomes smaller and smaller as the rapidly decreasing of the total deposited ion energy resulted from the decrease of ion velocity in the low-velocity region. At a critical ion velocity (v_c), the damage efficiency reaches a maximum ε_{max}, which corresponds to the turning point between these two stages.

ited energy density $D(r)$ is directly proportional to Z^{*2}. This means that the value of Z^* only influences the amplitude of the $D(r)$-r curve and does not influence the shape of the curve. Therefore, for a single ion-target system, the shape of the $D(r)$-r curve only depends on the value of ion velocity. If we normalize the $D(r)$-r curve, in other words, if we only consider the radial distribution of deposited energy density for a unit of stopping power, the $D(r)$-r curve is exactly the same for the same ion velocity even though the ion effective charge is different. This means that the damage efficiency, or the damage cross section per unit stopping power, should be free from the change of the ion effective charge. The change of damage efficiency along the ion penetration path is only due to the change of ion velocity. Therefore, the ε-ν curve is an ideal curve for investigating the influence of ion velocity on the irradiation damage process in a single ion-target system.

IV. CONCLUSIONS

Instead of the multiple ion-target irradiation system usually used before, in this study we used a single ion-target irradiation system and measured a series of damage cross section data along the ion path by using a continuous cross-sectional HREM observation method. By studying the changing relation of damage efficiency with the ion velocity, we further removed the influence of ion effective charge on the irradiation damage process and finally revealed a pure influence of ion velocity on the irradiation damage process.

On the curve of damage efficiency versus ion velocity for a single ion-target irradiation system Au-Bi-$Sr_2CaCu_2O_x$ we clearly see that the damage efficiency increases as the ion velocity increases in the low velocity region. When the ion velocity reaches about $0.057c$, the damage efficiency reaches a peak value. After that, the damage efficiency will decrease as the ion velocity increases further.

Both from the viewpoint of the threshold of dE/dx and from the viewpoint of radial distribution of deposited energy density, we have given an explanation for the changing relation of damage efficiency with the ion velocity. Two stages in the irradiation damage process have been suggested in this study. One is ion velocity controlled stage in the high ion velocity region. In this stage, as the ion velocity increases, the probability of the excitation of the high-energy second electrons will be higher. Since these high-energy second electrons usually go far from the ion path, the energy carried by them will have no contribution for producing the localized damage in the target material. Therefore the damage efficiency will become lower for a higher ion velocity in the high ion velocity region. The second stage is in the low ion velocity region, which is mainly controlled by the threshold for the energy density to produce permanent damage in the target. As the ion velocity decreases, the part of the deposited ion energy used to overcome the energy density threshold will become larger and larger. As a result, the damage efficiency will lower and lower. Due to the fact that the changing relations of the damage efficiency with ion velocity in the two stages are completely contrary, inevitably, a peak value of the damage efficiency will appear at the turning point between two stages.

ACKNOWLEDGMENTS

The authors would like to acknowledge S. Okayasu, T. Aruga, and K. Hojou for their kind collaboration in the ion irradiation experiments. They also would like to thank T. Hirayama, at the Japan Fine Ceramics Center, for his strong support in this research. Further thanks are due to Dr. Jun Yuan at the Cavendish Laboratory, the University of Cambridge for his helpful discussion and suggestion of the mechanism analyses. This work was partially supported by the New Energy and Industrial Technology Development Organization (NEDO) through the International Superconductivity Technology Center (ISTEC).

*Corresponding author. Electronic address: dxhuang@iname.com

[1] V. Hardy, D. Groult, M. Hervieu, J. Provost, B. Raveau, and S. Bouffard, Nucl. Instrum. Methods Phys. Res. B **54**, 472 (1991).

[2] L. Civale, A. D. Marwick, T. K. Worthington, M. A. Kirk, J. R. Thompson, L. Krusin-Elbaum, Y. Sun, J. R. Clem, and F. Holzberg, Phys. Rev. Lett. **67**, 648 (1991).

[3] M. Konczykowski, F. Rullier-Albenque, E. R. Yacoby, A. Shaulov, Y. Teshurun, and P. Lejay, Phys. Rev. B **44**, 7167 (1991).

[4] V. Hardy, J. Provost, D. Groult, M. Hervieu, B. Raveau, S. Durcok, E. Pollert, J. C. Frison, J. P. Chaminade, and M. Pouchard, Physica C **191**, 85 (1992).

[5] W. Gerhäuser, G. Ries, H. W. Neumüller, S. Schmidt, O. Eibl, G. Saemann-Ischenko, and S. Klaumünzer, Phys. Rev. Lett. **68**, 879 (1992).

[6] C. J. van der beek, M. Konczykowski, V. M. Vinokur, T. W. Li, P. H. Kes, and G. W. Crabtree, Phys. Rev. Lett. **74**, 1214 (1995).

[7] V. Hardy, A. Ruyter, A. Wahl, A. Maignan, D. Groult, J. Provost, Ch. Simon, and H. Noël, Physica C **257**, 16 (1996).

[8] H. Watanabe, B. Kabius, K. Urban, B. Roas, S. Klaumümzer, and G. Saemann-Ischenko, Physica C **179**, 75 (1991).
[9] B. Chenevier, S. Ikeda, H. Kumakura, K. Togano, S. Okayasu, and U. Kazumata, Jpn. J. Appl. Phys., Part 2 **31**, L777 (1992).
[10] Y. Zhu, Z. X. Cai, R. C. Budhani, M. Suenaga, and D. O. Welch, Phys. Rev. B **48**, 6436 (1993).
[11] J. Wiesner, C. Troeholt, J.-G. Wen, H.-W. Zandbergen, G. Wirth, and H. Fuess, Physica C **268**, 161 (1996).
[12] F. Studer, D. Groult, N. Mguyen, and M. Toulemonde, Nucl. Instrum. Methods Phys. Res. B **19-20**, 856 (1987).
[13] M. Toulemonde, G. Fuchs, N. Nguyen, F. Studer, and D. Groult, Phys. Rev. B **35**, 6560 (1987).
[14] D. Groult, M. Hervieu, N. Nguyen, F. Studer, and M. Toulemonde, Defect Diffus. Forum **57**, 391 (1988).
[15] M. Toulemonde and F. Studer, Philos. Mag. A **58**, 799 (1988).
[16] F. Studer, C. Houpert, D. Groult, and M. Toulemonde, Radiat. Eff. Defects Solids **110**, 55 (1989).
[17] J. M. Costantini, J. L. Flament, D. Groult, L. Sinopoli, F. Studer, M. Toulemonde, J. Trochon, and J. L. Uzureau, Radiat. Eff. **110**, 193 (1989).
[18] C. Houpert, F. Studer, D. Groult, and M. Toulemonde, Nucl. Instrum. Methods Phys. Res. B **39**, 720 (1989).
[19] F. Studer, C. Houpert, H. Toulemonde, and E. Dartyge, J. Solid State Chem. **81**, 238 (1991).
[20] F. Studer, C. Houpert, H. Pascard, R. Spohr, J. Vetter, J. Y. Fan, and M. Toulemonde, Radiat. Eff. Defects Solids **116**, 59 (1991).
[21] A. Meftah, N. Merrien, N. Nguyen, F. Studer, H. Pascard, and M. Toulemonde, Nucl. Instrum. Methods Phys. Res. B **59**, 605 (1991).
[22] F. Studer and M. Toulemonde, Nucl. Instrum. Methods Phys. Res. B **65**, 560 (1992).
[23] J. M. Costantini, F. Brisard, J. L. Flament, A. Meftah, M. Toulemonde, and M. Hage-Ali, Nucl. Instrum. Methods Phys. Res. B **65**, 568 (1992).
[24] J. M. Costantini, F. Ravel, F. Brisard, M. Caput, and C. Cluzeau, Nucl. Instrum. Methods Phys. Res. B **80-81**, 1249 (1993).
[25] A. Meftah, F. Brisard, J. M. Costantini, M. Hage-Ali, J. P. Stoquert, F. Studer, and M. Toulemonde, Phys. Rev. B **48**, 920 (1993).
[26] M. Toulemonde, S. Bouffard, and F. Studer, Nucl. Instrum. Methods Phys. Res. B **91**, 108 (1994).
[27] H. Dai, S. Yoon, J. Liu, R. C. Budhani, and C. M. Lieber, Science **265**, 1552 (1994).
[28] P. Hansen and H. Heitmann, Phys. Rev. Lett. **43**, 1444 (1979).
[29] A. Timm and B. Strocka, Nucl. Instrum. Methods Phys. Res. B **12**, 479 (1985).
[30] D. X. Huang, Y. Sasaki, S. Okayasu, T. Aruga, K. Hojou, and Y. Ikuhara, Phys. Rev. B **57**, 13 907 (1998).
[31] W. H. Barkas, *Nuclear Research Emulsions—I. Techniques and Theory* (Academic, New York, 1963).
[32] T. Aruga, K. Nakata, and S. Takamura, Nucl. Instrum. Methods Phys. Res. B **33**, 748 (1988).
[33] D. X. Huang (unpublished).
[34] M. Toulemonde, N. Enault, J. Y. Fan, and F. Studer, J. Appl. Phys. **68**, 1545 (1990).
[35] M. Leghissa, T. Schuster, W. Gerhäuser, S. Klaumünzer, M. R. Koblischka, H. Kronmüller, H. Kuhn, H. W. Neumüller, and G. Saemann-Ischenko, Europhys. Lett. **19**, 323 (1992).
[36] H. Kumakura, H. Kitaguchi, K. Togano, H. Maeda, J. Shimoyama, S. Okayasu, and Y. Kazumata, J. Appl. Phys. **74**, 451 (1993).
[37] R. Katz and E. J. Kobetich, Phys. Rev. **186**, 344 (1969).
[38] C. X. Zhang, D. E. Dunn, and R. Katz, Radiat. Prot. Dosim. **13**, 215 (1985).
[39] M. P. R. Waligórski, R. N. Hamm, and R. Katz, Nucl. Tracks Radiat. Meas. **11**, 309 (1986).